A STUDY OF THE CREATION AND CHARACTERIZATION OF NITROGEN DOPED $CUINSE_2$ (CIS:N), AS A POTENTIAL IMPROVED BACK CONTACT MATERIAL FOR CDTE AND $CU(IN_XGA_{1-X})SE_2$ PHOTOVOLTAIC CELLS

BY

THOMAS G. ERICKSON

THESIS

Submitted in partial fulfillment of the requirements
for the degree of Master of Science in Materials Science and Engineering
in the Graduate College of the
University of Illinois at Urbana-Champaign, 2016

Urbana, Illinois

Adviser:

Professor Angus Alexander Rocket

ABSTRACT

Nitrogen is incorporated into CuInSe2 (CIS), and other related materials, using a scalable, commonly used, technique. The growth characteristics, film morphology and electronic properties of these N doped materials, as it is affected by nitrogen, are studied, both in films grown with nitrogen, and in films implanted with nitrogen.

Dedicated to my family

Table of Contents

CHAPTER 1

INTRODUCTION

1.1 Motivation

Global climate change as a result of greenhouse gas emissions is a widely recognized problem facing humanity. At the same time developing countries are looking for ways to deliver electricity to an ever expanding population in ways that are both carbon neutral, and distributed, allowing them to skip expensive grid infrastructure. Solar power technologies, and specifically photovoltaics, are poised to fill these needs. Photovoltaics (PV) is a rapidly growing technology and is being deployed in record numbers across the globe. Each year the area covered by PV, the production capacity for PV, and the efficiencies of PV are all increasing while manufacturing and installation costs drop[1].

1.2 Goal

This thesis is a study of the creation and characterization of nitrogen doped $CuInSe_2$ (CIS:N), $CuGaSe_2$ (CGS:N) and $AgInSe_2$ (AIS:N), tolearn about N doping of CIS in general. The research determines dopant concentrations as a function of growth conditions and dopant supply, and measures changes to film morphology and composition. My work evaluates the electronic properties of the films, particularly looking at resistivity. I also explore the potential of other materials with an initial look into nitrogen doping in $AgInSe_2$ and $CuGaSe_2$.

CIS:N is an attractive material as a back contact to thin film photovoltaics for several reasons: 1. As a back contact in CIGS solar cells with higher p-type dopant levels, this will act to increase the built in electric field in the CIGS absorber layer. A similar method has been

demonstrated already in more easily doped Si cells[2]. 2. CdTe has a very high electron affinity which has made it difficult to make a good ohmic contact. The common solution to the contact problem is to dope the back surface of the CdTe with Cu. CIS:N could act as an intermediate layer, reducing the barrier height significantly, and also act as a stable source of Cu for the CdTe layer. CdTe devices typically rely on a small amount of Cu doping near the back contact to improve conduction of charge carriers, but simple metallic compounds or Cu doped graphite diffuse more and more Cu into the CdTe over time. CIS:N can also be alloyed with other materials, such as a Sulfur – Selenium substitution to match the valence band of the CdTe more closely[3]. 3. CIS:N can also potentially be used in non-PV applications. CIS has already been used to create simple diodes and transistors[4], [5], but more complicated electronic devices could be fabricated with the better, more controlled, p-type doping of CIS:N. This could include tunnel junction diodes and electronics printed on flexible low temperature substrates, at low cost.

A good understanding of CIS:N could allow nitrogen to be used in over chalcopyrites. The chalcopyrite system, having a I-III-VI_2 composition, includes materials with much wider bandgaps, which could be used as transparent conductors. Transparent conductors represent a wide variety of materials used in computer screens and PV amongst other applications, but most are n-type[6]. Nitrogen doped chalcopyrites could be a good p-type transparent conductor, if their bandgap was wide enough and if sufficient doping levels can be achieved reproducibly. In combination with n-type transparent materials it would be possible to create entirely transparent electronic systems as well.

CHAPTER 2

BACKGROUND

2.1 Background

Photovoltaics research in recent years has focused on a wide variety of aspects, but arguably the most important one is the efficiency of solar to electrical energy conversion. With improved efficiency comes reduced cost, per unit of energy produced, of installation, land usage and general balance of systems. As manufacturing costs have dropped in recent years, efficiency has become a larger limitation in the adoption of solar power.

Crystalline silicon (c-Si) represents the majority of the current PV market, as both the oldest and most developed type of solar cell, but has challenges moving forward. C-Si costs and efficiencies have improved over time[7]. However, they are rapidly reaching a point of diminishing returns. C-Si module efficiencies are approaching their theoretical limit[8], [9], and costs are being limited by the energy intensive refining processing and high purity required[10]. To continue improving PV technologies it is necessary to move to different material systems.

Second generation PV, so called thin film technologies, represent the best opportunity to realize those improvements. The two main thin film technologies are CdTe and $Cu(In_xGa_{1-x})Se_2$ (CIGS), and make up almost all of the remaining PV power market[1]. Both have higher theoretical efficiencies than Si, due to having a more ideal direct band gap. Thin film technologies are also able to be manufactured much more quickly, inexpensively, with simpler

precursor materials[11], and can be deposited on a variety of low cost, light and sometimes flexible substrates. The latter make both roll to roll continuous production possible and installation easier and available in more locations, such as unreinforced roof tops. CdTe and CIGS PV have also been around for a long time, allowing for extensive study and a proven track record of reliability, unlike many newer technologies such as organic or perovskite PV.

While all of the previous facts about CdTe and CIGS might make them seem like perfected technology, many aspects of thin film PV cells are either less than ideal, or poorly understood. In fact, while CdTe and CIGS both have high theoretical efficiencies, the actual observed efficiencies are consistently lower than those of c-Si, with record cell efficiencies measured at 22.1% (CdTe) and 22.3% (CIGS) compared to c-Si efficiency of 25.0%[7]. One particular aspect that can be improved, with better materials, is the back contact of these devices. In CdTe devices the back contact is typically a copper containing metallic layer, which results in both a large Schottky barrier[12] and copper diffusion over time into the CdTe layer[13]. Both of these mechanisms reduce the overall efficiency and lifetime of CdTe PV. CIGS back contacts are usually Mo with a thin $MoSe_2$ layer[14], which forms a good site for charge recombination, leading to loss in efficiency. The typical solution to this is a band gap grading of the CIGS near the back contact[15], which results in a less than ideal absorption profile and depletion region in the device.

Thin film PV cells have a heterojunction structure and are constructed with a back contact, formed of a metal layer, then the main p-type absorber layer (either CdTe or CIGS), then n-type CdS (or other similar wide-gap n-type semiconductor), and finally a transparent conductor, typically Al doped ZnO. The structure is shown in figure 2.1. In CIGS devices the

absorber layer is generally thought to be converted to n-type near the CdS layer due to Cd infiltration into the CIGS [16]. CdTe is made heavily p-type near the back contact by indiffusion of Cu from the back contact, which helps lower the back contact barrier[13]. CIGS cells often have band gap grading with increased Ga at the rear of the absorber layer[15] to reduce minority carrier recombination at the back contact. Many of the recent improvements in efficiency have come from improved process control and better material quality, and a thinning of the CdS layer in both CIGS[17], and CdTe[18] devices. Improvements to CdTe cells over the past 5 years have mostly improved carrier collection[19], [7]. No real change to back contact structure or processing for CIGS cells has occurred recently[20].

CIS:N and relatively wider gap chalcopyrites are attractive materials to provide the back contact of thin film photovoltaics because of its ability to be grown in a variety of conditions and processing techniques. $CuInSe_2$ (CIS) and related materials, very generally $(Cu_{1-x}Ag_x)(In_{1-y}Ga_y)VI_2$ (VI = S, Se, Te) alloys, have been grown on glass[21], steel[22] and polymer[23] substrates, while maintaining good optical and electronic properties. It has been grown by evaporation[21], sputtering[24] and annealing of metal films in a Se atmosphere[25]. Stoichiometric CIGS stable up to 800°C[26], while deposition at lower temperatures also yields good material[27].

Defects in these highly ionic semiconductors either form neutral defect clusters, or (for polycrystals) migrate to grain boundaries and disappear, leaving carrier mobilities and lifetimes relatively high[28]. The bandgap of chalcopyrites is direct and tunable over a wide range, from 0.95 eV for $CuInTe_2$ [29] and 1.04 eV for $CuInSe_2$ to 2.67 eV for $AgGaS_2$[30]. In addition, the energy of the conduction and valence bands can be shifted independently through changes to

anion and cation chemistry. In the case of creating back contacts to CdTe, alloying $Cu(In,Ga)Se_2$ with $Cu(In,Ga)S_2$[3], the valence band can be shifted to be close to the valence band of CdTe.

CIS has largely been studied with samples that have not been intentionally doped. This undoped material is generally lightly p-type. Large single crystal CIS grown with the Bridgeman technique has typical p-type carrier concentrations at room temperature of 10^{18} carriers/cm^3 with carrier mobility on the order of 200 cm^2/V s[31]–[33]. However, these fairly large carrier concentrations and mobilities have not been adequately explained and have not been observed in polycrystalline thin films. Polycrystalline thin films, similar to record solar cell device material, show much lower cross grain mobilities on the order of 5 cm^2/V s and carrier concentrations at around 10^{15} carriers/cm^3 [34]to 10^{18} carriers/cm^3 [35] in very large grain films. Behavior similar to that of bulk crystals has been observed in epitaxial films grown on GaAs, with high mobilities and carrier concentrations[36]. In some cases, lower mobilities similar to polycrystalline films is observed in epitaxial films[37], [38]. In one study, much higher carrier concentrations, as high as $6x10^{20}$ carriers/cm^3, have been demonstrated in epitaxial films of CGS, without a significant loss in mobility, indicating that the conductivity of the chalcopyrite films can be greatly enhanced[39].

The most commonly studied extrinsic impurity in CIS, and one that was be used in some films for this study, is Na. Na is present in all record efficiency solar cells. The removal of Na has been shown to decrease the efficiency of CIGS cells[40]. If CIS:N is going to be effective in CIGS solar cells it will have to perform with Na present. Na has been demonstrated to have several effects in CIS films. In Se rich films, it increases the majority carrier concentration by reducing compensating defects[41]. This effect may be important in creating p+ CIS:N. In Se

poor films Na has been shown to change the majority carrier type from p-type to n-type[31]. It has also been proposed that Na helps to passivate grain boundaries in CIS[42]. The films in this study were be grown on substrates that are both Na free and Na containing.

Experiments have already shown that N can be used as a p-type dopant in CIS films grown with molecular beam epitaxy. These films were grown on quartz substrates at temperatures from 500°C to 475°C[43]. Cu, In and Se were supplied with individual evaporation cells, while N^+ ions were implanted at an energy of 10 keV and an area density of $5*10^{17}$ cm^{-2}. A later study by the same group used a radical N source, formed a magnetically contained plasma, with an accelerating voltage from 50-150 volts, with controlled ion current[44]. Films had resistivities below 1 ohm-cm for ion implantation and 66 ohm-cm for samples grown with a radical N source, 2-3 orders of magnitude lower than typical for polycrystalline films. These studies did not measure carrier concentrations or mobilities directly, though all films with N were observed to be p-type.

A similar semiconductor, ZnSe, has also shown enhanced p-type conductivity with N doping[45]. ZnSe has a wider band gap than CIS, but has a similar crystal structure, lattice constant and direct bandgap. With the valence band of both materials dominated by Se 4p orbitals, both materials should show similar extrinsic p-type doping by the same elements. N doping of ZnSe has been done through the addition of diluted N_2 gas in Ar in a RF plasma[46]. This doping was done to ZnSe on a GaAs wafer substrate, and doping was achieved up to 10^{16} cm^{-3} at a low activation energy. Density functional theory has been used to predict that N sits on a Se site in ZnSe[47], which is relevant in the CIS system because if N sits on a similar site in the chalcopyrite lattice, it will contribute one less valence electron, yielding p-type doping.

2.2 Figures

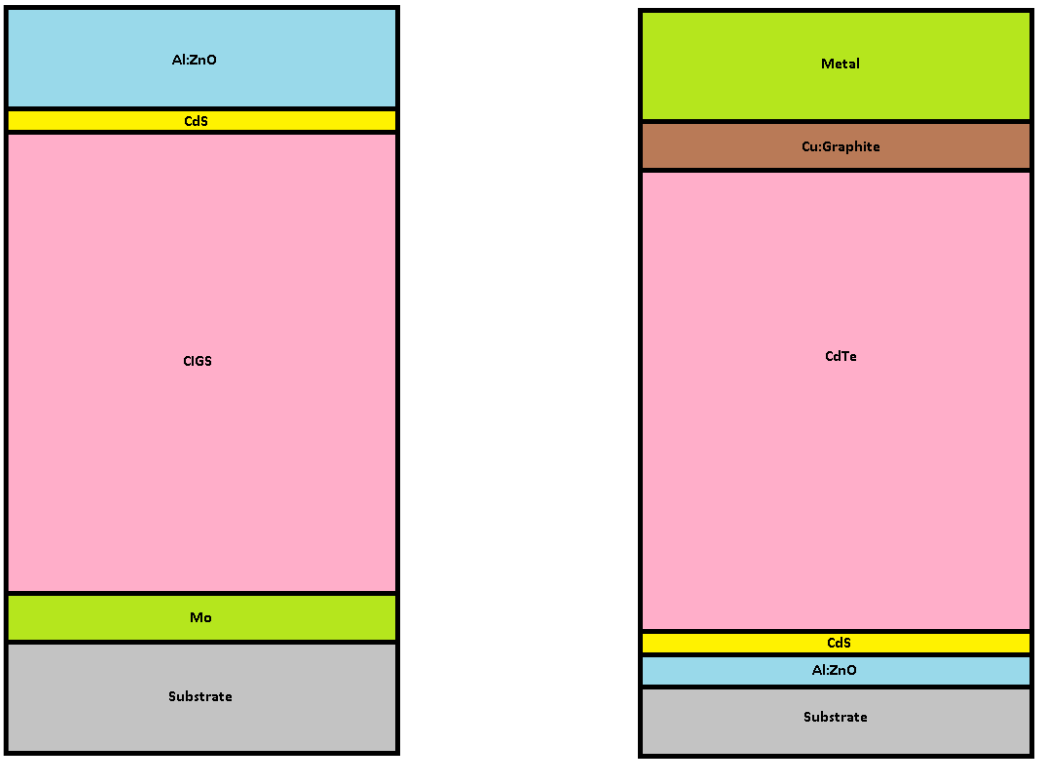

Figure 2.1: Thin film PV cell typical structure. CIGS is illuminated from the top, while CdTe is illuminated from the bottom.

CHAPTER 3

EXPERIMENTAL METHODS

3.1 Sample Growth

CuInSe2 films were grown using a hybrid sputtering and evaporation technique described in detail in Reference[48], [49]. The deposition chamber base pressure is typically $7x10^{-4}$ Pa. Metallic Cu and In targets are dc magnetron sputtered independently in a 0.27 Pa sputtering gas, typically Ar, in the presence of a Se flux from an effusion cell. The sputtering currents on the Cu and In targets are controlled to achieve the desired film stoichiometry. The Se cell is initially heated to a set point of 520°C to accelerate heating of the Se, then after 5 minutes the set point is reduced to 320°C for the duration of the growth for the desired deposition rate of approximately 40 nm/min. The sputtering sources are separated from the substrate during growth by 25 cm, while the evaporation cells sit 18 cm from the substrate. This configuration allows material from the sputtering targets to be thermalized by the time it reaches the substrate, since the mean free path for low energy species in the sputter gas is around 6 cm. The substrate is clipped to a resistive heater. Temperature is measured both with a thermocouple attached to the heater and using a pyrometer to measure the substrate temperature directly. In the case of glass substrates, temperature is measured after 5 minutes of growth to allow a thin film to form.

Three substrates were used for the growth of films. Polished (100) oriented GaAs is used to grow epitaxial CIS films. Epitaxial films are of interest to this study because they eliminate the complicating effect of grain boundaries and generally exhibit much higher in

plane carrier mobilities than polycrystals. Films grown on soda lime glass substrates were also studied as this material is commonly used as a substrate in high efficiency and commercial CIS devices. Soda lime glass has a thermal expansion coefficient similar to CIS, and it contains Na, that diffuses into the film during growth. Na is typically found to improve device performance. However, soda lime glass is limited by its low glass transition temperature of 573°C, which sets an upper limit on growth temperature. Single crystal Si with only the native oxide, is used as the third substrate to grow polycrystals at elevated temperatures without Na. Films grown on glass were deposited at 580°C, while films grown on GaAs and Si were deposited at 680°C.

N was introduced during growth by adding N_2 to the Ar sputtering gas, keeping the overall pressure constant. The relative partial pressures of N_2 and Ar are controlled with needle valves and ultra-high purity (99.99% purity) gases are used.

N was also introduced to films after growth using ion implantation. Five films grown without any N, and slightly Cu poor, have been implanted at an energy of 400 keV and a dose of $5x10^{15}$ cm^{-2}. This led to a projected range of 500 nm, in 700 nm thick films. This depth was selected to result in the bulk of the implanted atoms remaining inside the film and yields a volumetric density of 10^{20} cm^{-3}. A simulated implant profile is shown in figure 3.1.

Thin films were also grown using slightly different materials. By switching sputtering targets, $AgInSe_2$ (AIS) and $CuGaSe_2$ (CGS) were grown with varying amounts of nitrogen. AIS was grown using pure elemental Ag and In targets. CGS was grown using a pure Cu target and a 30% Cu, 70% Ga sintered target. AIS and CGS are similar to CIS, while having larger band gaps (1.24 eV for AIS and 1.68 eV for CGS).

3.2 Sample analysis

Samples were analyzed for composition, morphology and electrical properties. It is important that new phases are not formed by the introduction of N, while achieving the desired doping effects.

Structural characterization was done initially through secondary electron imaging (SEI) in a scanning electron microscope (SEM). The SEM was a JEOL 7000F field emission SEM using a 20 keV beam at 500 pA and 10kx magnification. While the SEI derived information is largely qualitative it gives a good estimate for grain size, film thickness and general film structure. X-ray diffraction (XRD) was the primary tool for detecting possible second phases created by the addition of N, as well as detecting changes in average grain orientation. The instrument used was a Phillips X'pert diffractometer. The x-ray source was collimated Cu K_α radiation (λ=0.154 nm). ω-2θ scans were performed over a range of 10° to 90° with a step size of 0.05° and time of 2 seconds. Films grown on GaAs and Si were aligned to the substrate's <100> (GaAs) and <111> (Si) planes. The data was compared to powder diffraction files for peak positions and areas. XRD was especially important in establishing the epitaxial relationship between films grown on GaAs and the substrate.

Chemical characterization was done with complementary techniques of energy dispersive x-ray spectroscopy (EDS), x-ray photoelectron spectroscopy (XPS) and secondary ion mass spectroscopy (SIMS). EDS is a SEM-based technique that is quantitative, but has a limited elemental sensitivity, down to around 1 atomic percent (at%) and has difficulty detecting light elements. This made EDS useful in controlling the stoichiometry of the deposited compounds.

EDS can also be used to get rough approximations of the spatial distribution of elements, allowing mapping of elements across different parts of the films or as a function of depth. EDS was performed using the same conditions described for SEI, over ~10 µmx 10 µm square area. The Thermo Scientific EDS detector had a 35° takeoff angle. Quantification was done using a Phi-Rho-Z correction method [50]. The 20 keV beam energy allowed me to use Cu and Se K lines for quantification, eliminating interference in the L lines. There was some overlap between N k emission and In M lines, but analysis of the data showed no correlation between In content and observed N content. EDS results were used to quantify bulk film stoichiometry.

XPS gathers quantitative elemental information, similar to EDS, but is surface sensitive and more sensitive to lighter elements, like N. Chemical information is also available, indicating the bonding state of individual elements and fermi level. XPS was performed using a Kratos AXIS Ultra, with an Al x-ray source at 1.486 keV. Spot size was ~1mm x 1mm. Spectra were taken from 0 to 1100 eV.

SIMS has much higher sensitivities for most elements, collects some chemically sensitive information, and gives a much higher depth resolution. As a result SIMS was used for the detection of very small quantities of dopants, such as N and Na, and to detect changes in elemental concentrations as a function of film depth.

SIMS was performed with Cs and Au ion beams for sputtering and analysis respectively, over 50 µm x 50 µm square area in a PHI Thrift III time of flight (TOF) SIMS instrument. This dual beam system used Cs^+ ions to sputter material away in a larger 600 µmx 600 µm square area, and then a Au^+ beam was used for analysis. Analysis took 21 seconds and then sputtering

was carried out for 30 seconds. During analysis, negative ions were collected from 0 to 800 amu. This cycle was repeated until the substrate material was reached. Some samples had smaller amounts of N than could be detected with EDS. Because the SIMS detection sensitivity is typically consistent over a range of compositions the same scale factor could be used as was determined at higher concentrations. The overall trend of increasing N with N_2 gas during growth matched with the values observed in XPS, and allowed for quantification below XPS limits. In my experiemnts I used $Cs+N^-$ molecular ions (147 AMU) to detect N. Previous works have used $Se+N^-$ (94 AMU) which gives higher sensitivity but was not observed in the current experiments for reasons that were not clear.

Electronic characterization was done with a 4-point probe, hot point probe, Hall Effect and the Vander Pauw technique. Hot point probe and Hall Effect were used to establish carrier type. Hot point probe used nickel plated leads spaced 1 cm apart with one tip heated to ~300°C using a soldering iron. Hall Effect measurements were performed on samples grown on glass substrates with four In solder contacts made directly to the CIS. The contacts were roughly 1 mm in diameter on the corners of 1 cm^2 samples. Hall Effect measurements were performed in a 1 Tesla magnetic field, switching current directions, which leads were having current driven or voltage measured, and magnetic field directions. Four point probe and Vander Pauw established sheet resistance. Four point probe was performed with WC tips spaced 1 mm apart with a current of 10 μA. Vander Pauw measurements were performed using the same contacts as for Hall Effect without the presence of a magnetic field. After establishing the film thickness through cross sectional SEI, the relationship $\rho = t*R_s$ (where ρ is resistivity, t is film thickness, and R_s is sheet resistance) is used to calculate film resistivity, the most important factor in using

these materials as an electrical contact. Hall Effect is based on transverse voltage measured as a function of applied current (200 mA) in a magnetic field. Carrier concentrations can be derived from the equation $n = \frac{IB}{V_h et}$ (where n is carrier concentration, I is applied current, B is applied magnetic field, V_h is the transverse voltage, e is the charge of an electron, and t is the film thickness). The carrier concentration in turn is used to calculate carrier mobilities using the relation $\mu = \frac{1}{n\rho e}$, where μ is mobility, n is carrier concentration, ρ is resistivity and e is the charge of an electron.

3.3 Figures

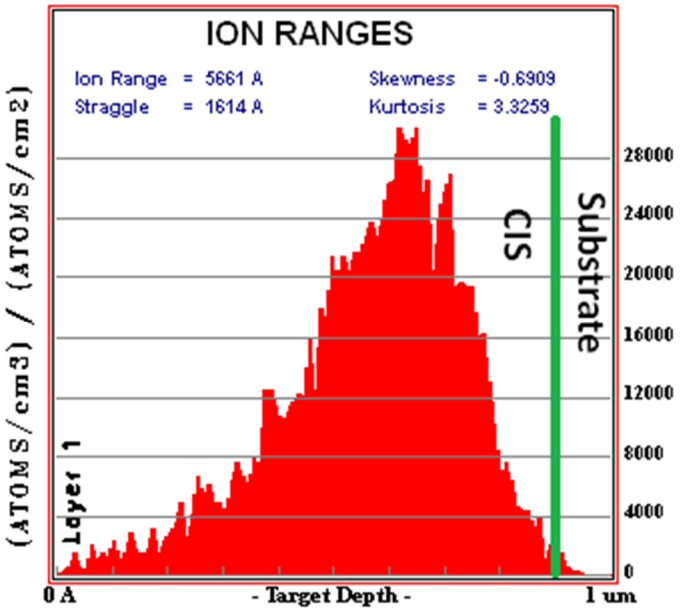

Figure 3.1: Ion implantation ranges, showing the calculated penetration depth of nitrogen into CIS

CHAPTER 4

RESULTS

4.1 Nitrogen Incorporation

I measured an increase in N exponentially with the N_2 partial pressure, shown in figure 4.1. The maximum measured concentration is around 10 at%, based on XPS, shown in figure 4.2. There was a corresponding linear decrease in Se, in a 1:1 ratio to the added N measured with EDS. These changes were observed in films grown on Si but not on glass, as shown in figure 4.3. This suggests that N is sitting on Se sites in the chalcopyrite lattice. Films grown on GaAs, and films of AIS, were more not analyzed with XPS. Nitrogen was detected in these films in SIMS, but large enough sample sizes were not available to establish any clear relationship with growth conditions.

EDS results also showed that Cu and In content varied. Adding N_2 reduced the In content in general, resulting in some cases in Cu-rich and highly conductive films (Figure 4.4). It was concluded that during start-up of the deposition process the In target surface may have been converted to InN. This problem was corrected through a 5 minute pre-sputter of the targets in pure Ar. With the pre-sputtering approach no change in film composition was observed under different N_2 fraction in the sputtering gas. This showed that no preferential sputtering of the substrate was occurring as a result of the change in gas content.

4.2 Morphology

SEI was used to confirm that the thin films grown on glass and Si were polycrystalline and formed from dense columnar grains. SEI showed epitaxial films on the GaAs substrates, with facets along (112) planes, similar to what has been seen previously[51]. Epitaxy was confirmed by XRD, as discussed below. Characteristic planview images are shown in Figure 4.5 for samples on the three different substrates. For these images the deposition conditions were as follows: All samples were grown in pure Ar, with the sample grown on glass heated to 580°C, and samples grown on GaAs and Si heated to 680°C. These images were used to estimate the grain size for films on Si at around 500 nm, and soda limes glass at around 250 nm, which is typical for CIS polycrystals. SEI also measured film thickness via fracture cross sections, which showed that growth rates were consistent across various nitrogen partial pressures, at 9.4±1.5 nm/min.

XRD analysis of the deposited films showed that the polycrystals grown on soda-lime glass showed a random orientation, consistent with standard powder diffraction on the material, for N_2 sputtering gas fractions up to ~0.4 (Figure 4.6) but showed a significant increase in the preferred (112) orientation for higher fractions of N_2. The films on Si showed a greater amount of (112) texture for zero and 100% N_2 in the sputtering gas with a general preference for (112) at intermediate N_2 levels (Figure 4.7). No evidence of the formation of amorphous or other second phases was found with N_2 addition. This indicates that no surface or grain-boundary segregated phases such as InN were present in the films. The peak positions do not change significantly with N_2 addition, which is surprising given the replacement of the large Se anions with much smaller N anions. However, it is clear that N_2 was incorporated and Se was lost so presumably other factors dominated the lattice constant. Analysis of the XRD peak

positions showed that the lattice constants were a=0.574±0.001 nm and c=1.155±0.002nm. This is ~0.4±0.3% smaller than the bulk lattice constants for CIS.

High quality epitaxial films could be grown on GaAs with up to 9% N_2 in the sputtering gas. High N_2 levels resulted in the formation of polycrystalline films, heavily oriented to the substrate but with some (112)-oriented grains appearing (see for example, Figure 4.8). Low levels of added N_2 appear to produce a more well-defined (400) epitaxial film peak without statistically-significant peak shifts. There is minor evidence of a shift to lower diffraction angle (larger lattice constant) with addition of N_2 but any shift is within the noise of the measurement. Furthermore there may have been a change in the migration of Ga out of the substrate, consistent with the clearer CIS peak with less intensity at the diffraction angles between CIS and GaAs.

The addition of N_2 to the sputtering gas during growth of AIS and CGS showed a lack of morphological change when grown on glass. SEM imaging of AIS was difficult due to the sample's high resistivity causing charging. Therefore no estimate of grain size could be made. XRD was not performed on the AIS and CGS films.

4.3 Increased p-type Conductivity with Nitrogen

Carrier concentration increased approximately exponentially in polycrystalline films by 4 orders of magnitude, with N_2 addition to the gas (Figure 4.9). For N_2 sputtering gas fractions above 0.6, films grown on glass continued to decrease in conductivity another 2 orders of magnitude, while films grown on Si did not grow less resistive. It is proposed that the presence of Na from the soda-lime glass was responsible for the continued decrease in conductivity at

the highest N_2 concentrations. However, the interaction of Na with the films was not determined. However, Na has been shown to reduce the effects of compensating donor defects in CIS films[41].

To determine if doping was occurring, XPS was performed to measure the peak positions for elemental core levels. These showed an overall peak shift of -26 to -38 meV at 50% N_2 gas fraction, and -50 meV at 100% N_2 gas fraction, for the Cu, In and Se peaks. This matches qualitatively with the expected fermi level change from increased p-type doping. The valence band was not measured.

For films grown on GaAs, no change in resistivity was observed with increasing N_2 as long as the films stayed epitaxial. At 10% N_2 gas fraction, where epitaxy is preserved, the expected change to resistivity is within the variability of different growths, and the amount of N detected by SIMS is in the background noise. At higher concentrations of N the films were no longer epitaxial, so direct comparisons to epitaxial material was less meaningful. Polycrystalline CIS:N grown on GaAs followed a very similar trend in resistivity to samples grown on Si, under similar conditions (Figure 4.10).

Hall effect measurements showed no change in carrier mobility in the polycrystalline films as a function of N_2 in the sputtering gas, although the mobilities were dominated by grain boundaries in the polycrystalline films. Mobilities in polycrystals were < 1 cm^2/Vs, which is not unusual for polycrystalline CIS films. This observation also suggests that no second phases were present in the grain boundaries, similar to the conclusion from the XRD results.

The percentage of N actively contributing acceptor states can be calculated by combining measured carrier concentrations with N concentration in the films. This is shown in figure 4.11, and changes from very low values to a few percent of nitrogen atoms adding acceptors. Because of the variation in the measured values no trend can be ascribed to the results, although Figure 4.11 is suggestive that the incorporated N is becoming more active as its concentration increases.

Implanted samples showed a significant reduction in resistivity, as shown in figure 4.12. Past experiments have shown that ion implantation of any element can reduce the resistivity of CIS [52],[39], although this varies significantly as the carrier mobility within the grains can also be reduced. Overall it appears very likely that the samples that were ion implanted showed a significant increase in conductivity.

4.4 CGS and AIS

Experiments on AIS and CGS were not as successful as those performed with CIS. AIS remained highly insulating at all levels of N_2 in the sputtering gas, to the point where current could not be pushed through 4 point probe leads, and static charge made SEI difficult. CGS did show some changes in conductivity, but without a clear dependence on N_2 content, as shown in figure 4.13.

4.5 CdTe contacts

CGS:N was deposited as a back contact to CdTe devices. The devices were made at the University of Toledo, and were complete except for the back contact. The contacts were a 4mm diameter circle of CGS deposited at 50% N_2 gas fraction. The resulting devices behaved as

a diode in the dark. However, under illumination they behaved as resistors with the addition of photocurrent generation (Figure 4.17). The best device had a fill factor of 0.25 and open circuit voltage of 0.6 V. However, the greatest loss seemed to be in carrier collection, which was > 100 times lower than when using a standard Cu/Au metallic contact on similar devices. The resulting I-V curves are shown in figure 4.17.

4.6 Figures

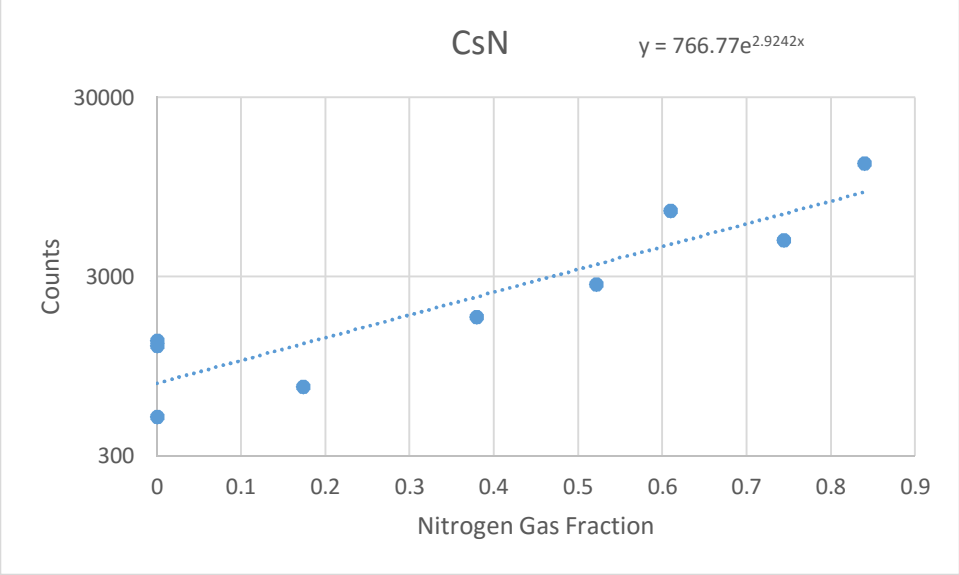

Figure 4.1: SIMS data also shows an increase in N content with increasing nitrogen gas fraction, allowing for better detection at small values of nitrogen. These films were grown on glass.

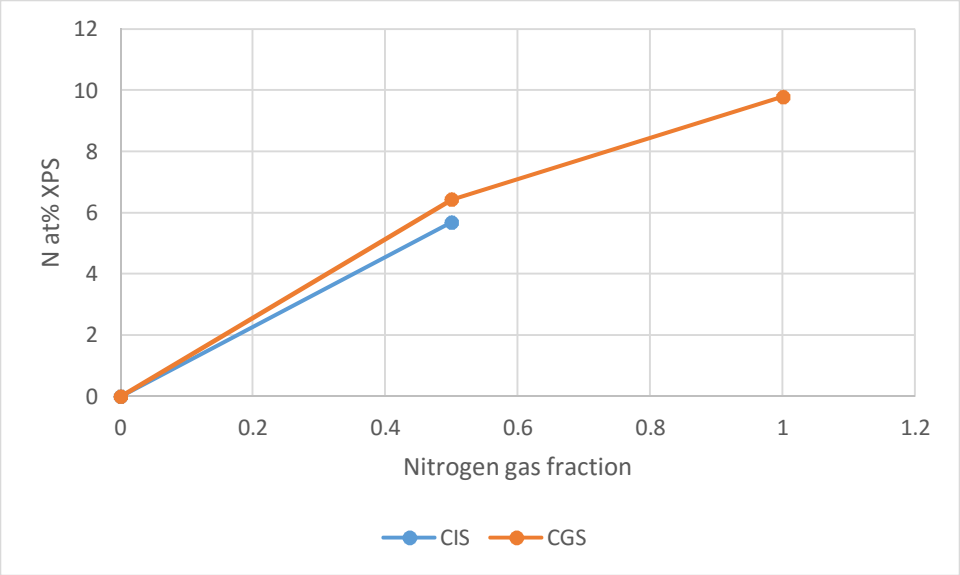

Figure 4.2: XPS data showing the increase in N as a function of N_2 gas during growth. These samples were CIS and CGS grown on glass

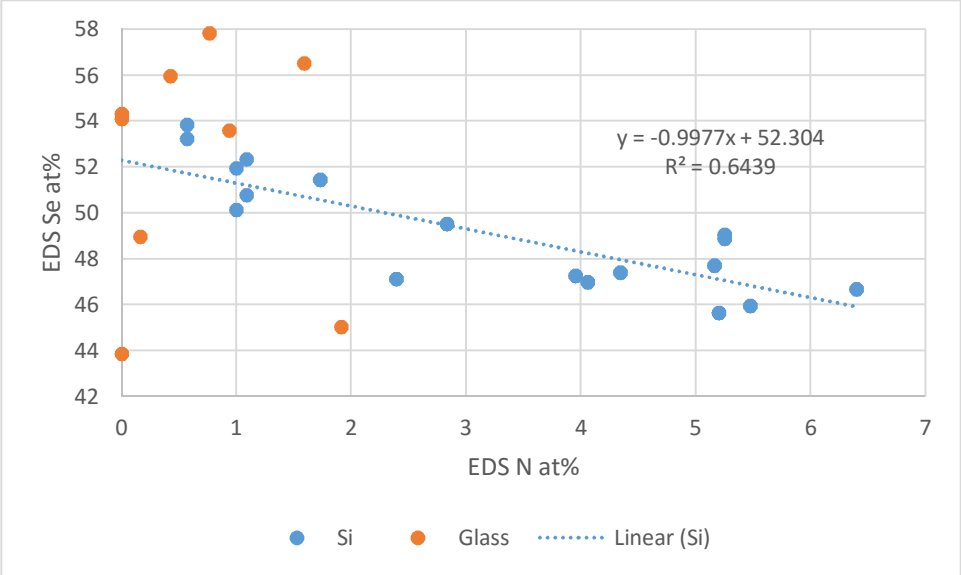

Figure 4.3: Se decreases with additional nitrogen content at almost exactly a 1:1 ratio in films grown on Si. The data shown here is for films grown on Si and glass.

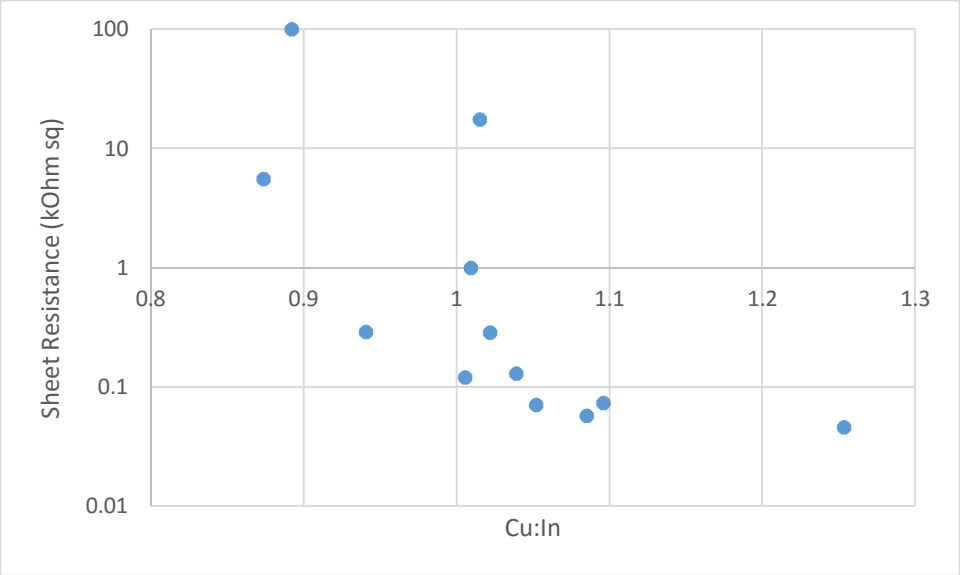

Figure 4.4: Resistivity change in CIS films grown without nitrogen as a function of Cu:In ratio

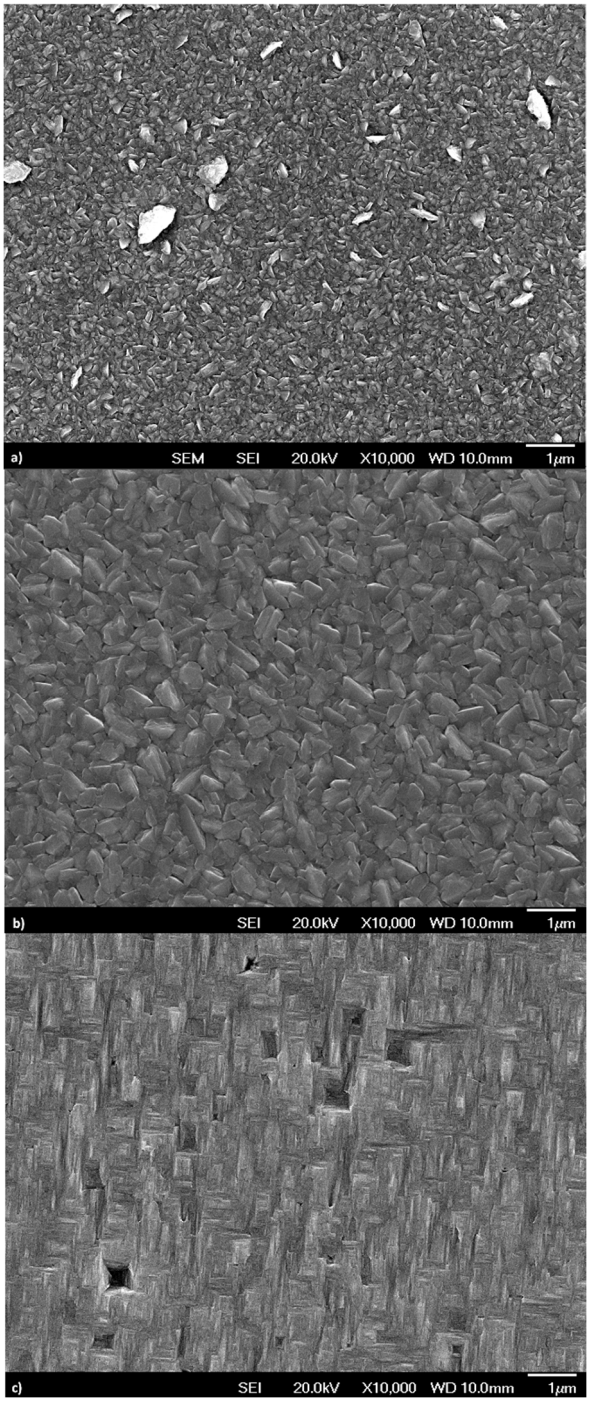

Figure 4.5: Planview SEI images of CIS films on a) soda lime glass, b) Si (111), c) GaAs (100)

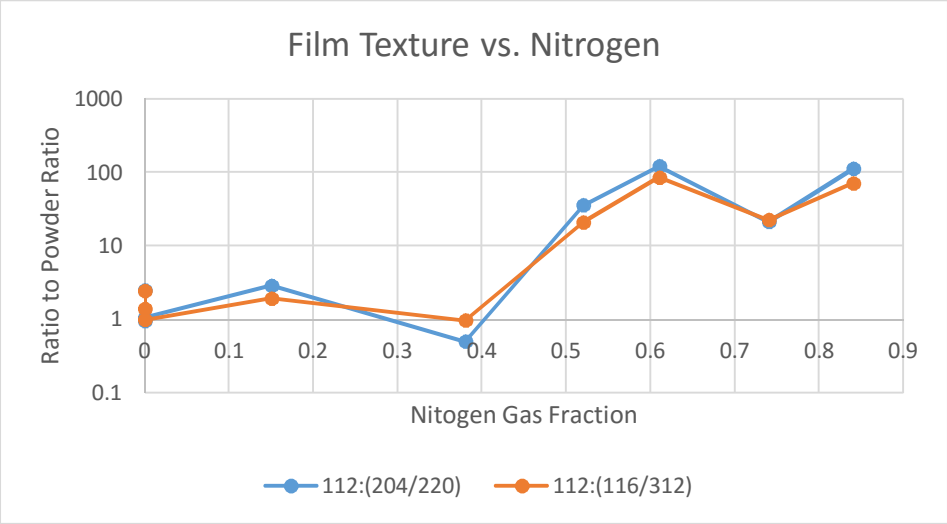

Figure 4.6: XRD peak areas, of films grown on soda lime glass, of the (112) peak is divided by either the (204/220) peak or the (116/312) peak, then compared to the expected powder diffraction values. The (112) peak is significantly larger then in a randomly oriented film in films grown with N.

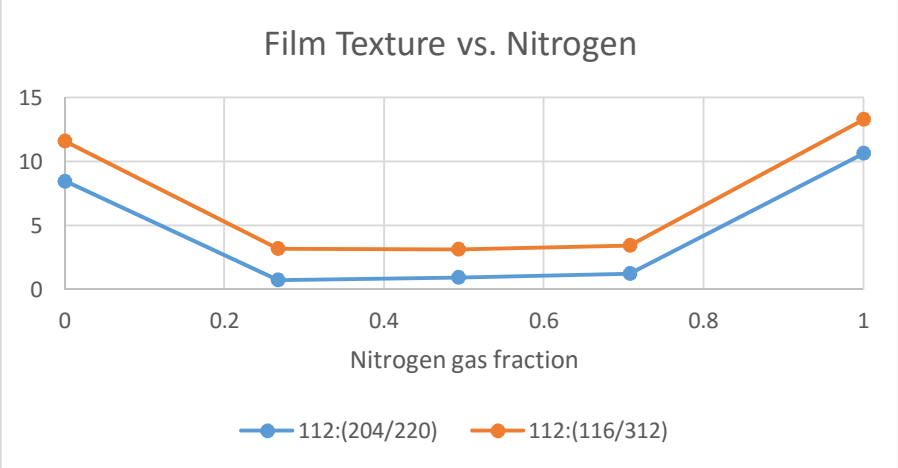

Figure 4.7: XRD peak areas, of films grown on Si, of the (112) peak is divided by either the (204/220) peak or the (116/312) peak, then compared to the expected powder diffraction values. The (112) peak is significantly larger then in a randomly oriented film in films grown with pure Ar or N.

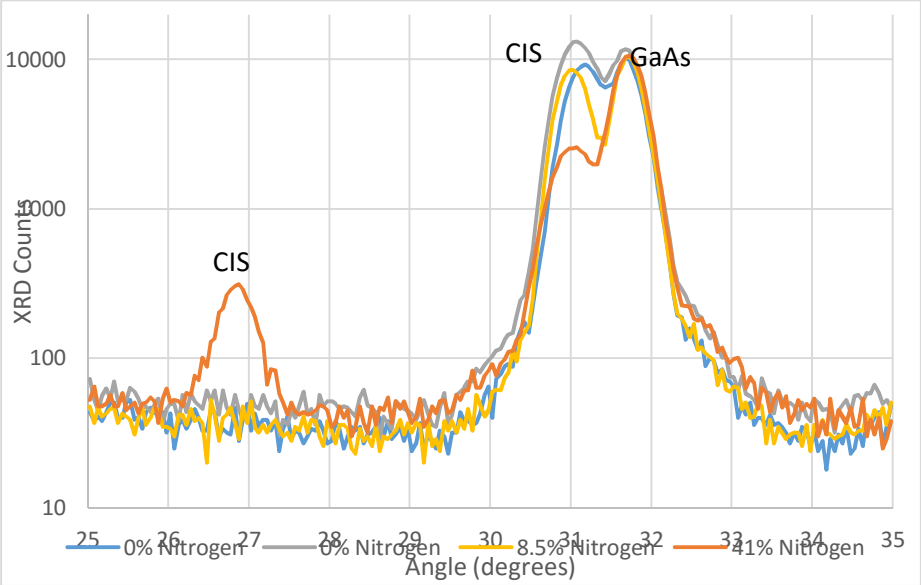

Figure 4.8: The disruption of epitaxy is shown in the decrease of the epitaxial (400) peak and the increase in the randomly oriented (112) peak, with increasing nitrogen gas fraction

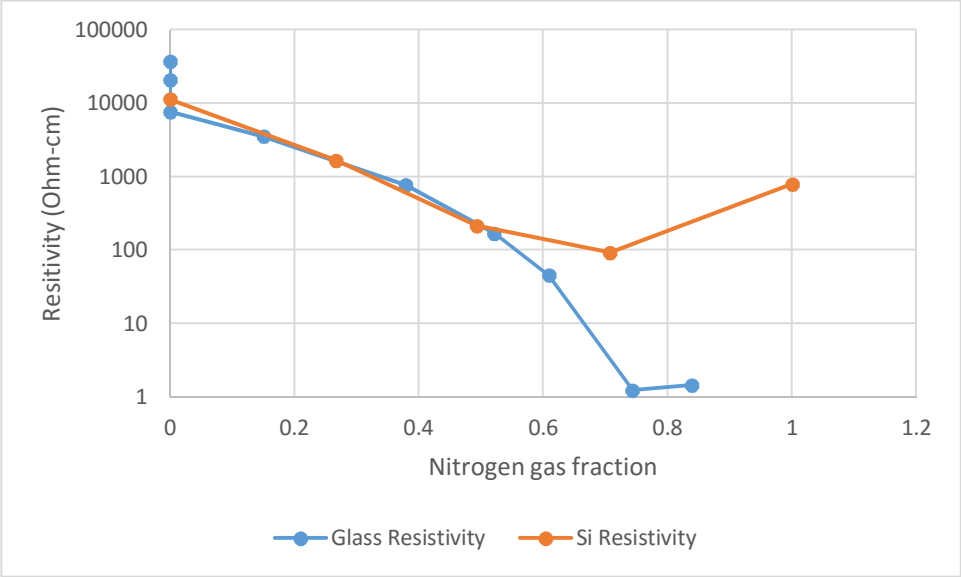

Figure 4.9: Resistivity of films drops several orders of magnitude on films grown on Glass and Si substrates. Films grown on glass drop to lower values.

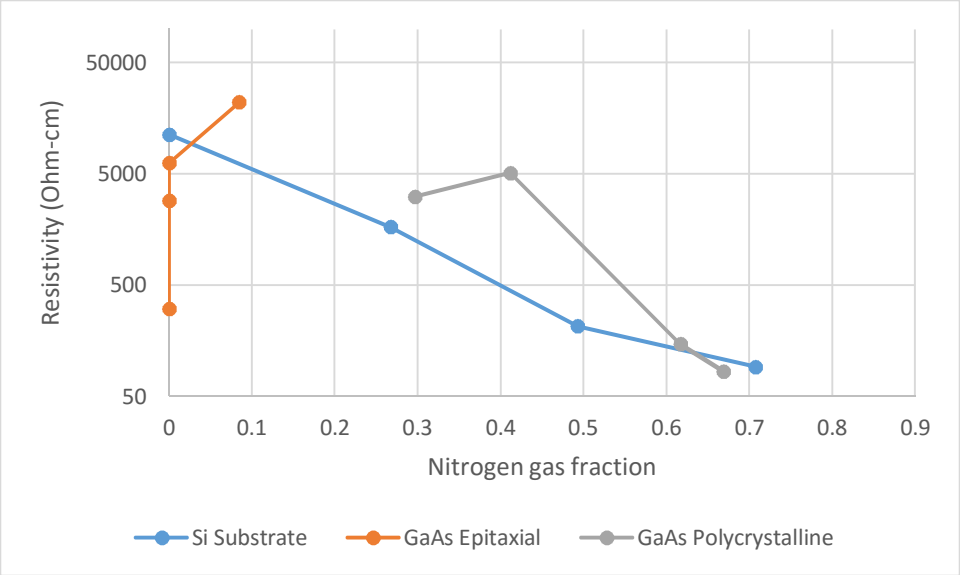

Figure 4.10: Epitaxial films grown on GaAs showed no decrease in resistivity with nitrogen. Polycrystalline films on GaAs did show a decrease, similar to films grown on Si.

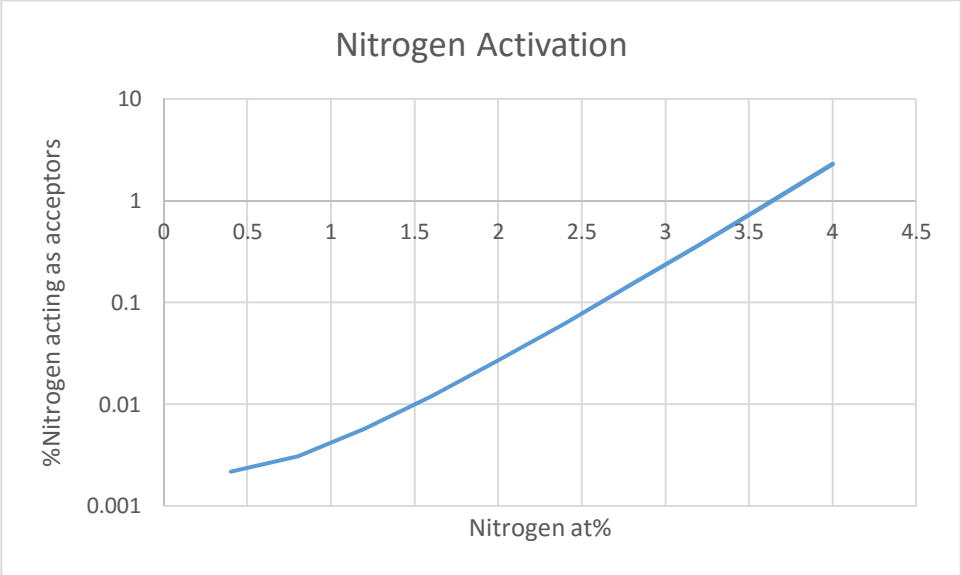

Figure 4.11: Combining nitrogen concentrations with electrical properties measured with Hall Effect and 4 point probe, the % of nitrogen atoms contributing charge carriers is calculated as a function of nitrogen at%

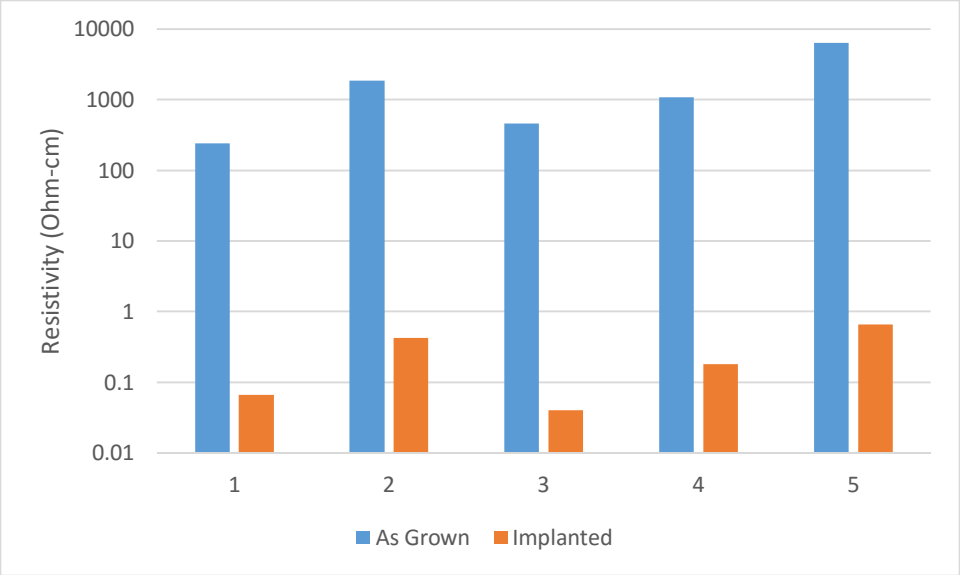

Figure 4.12: Polycrystalline film resistivity before and after ion implantation of nitrogen. Films were grown on soda-lime glass. Films were not annealed after implantation.

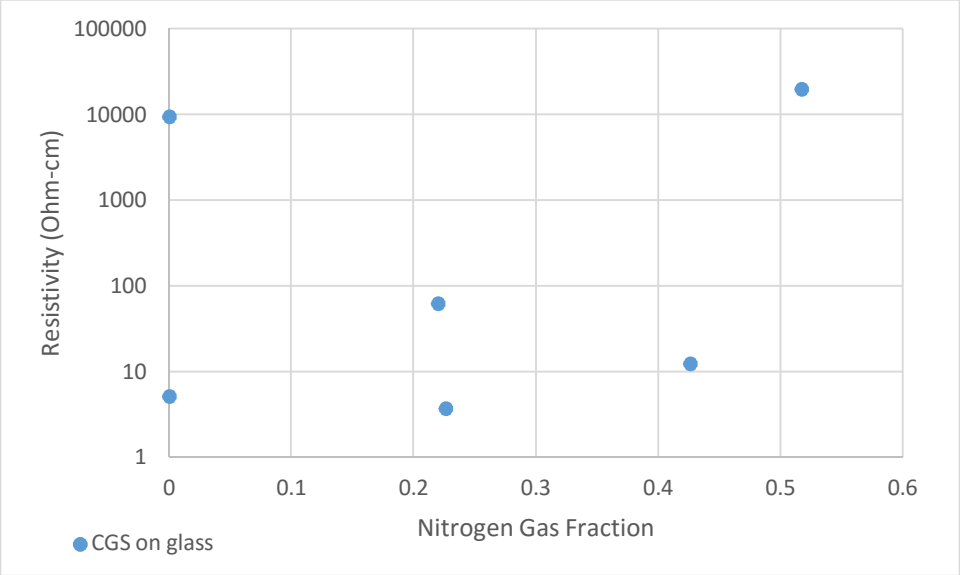

Figure 4.13: Resistivity as a function of nitrogen gas fraction during growth in CGS

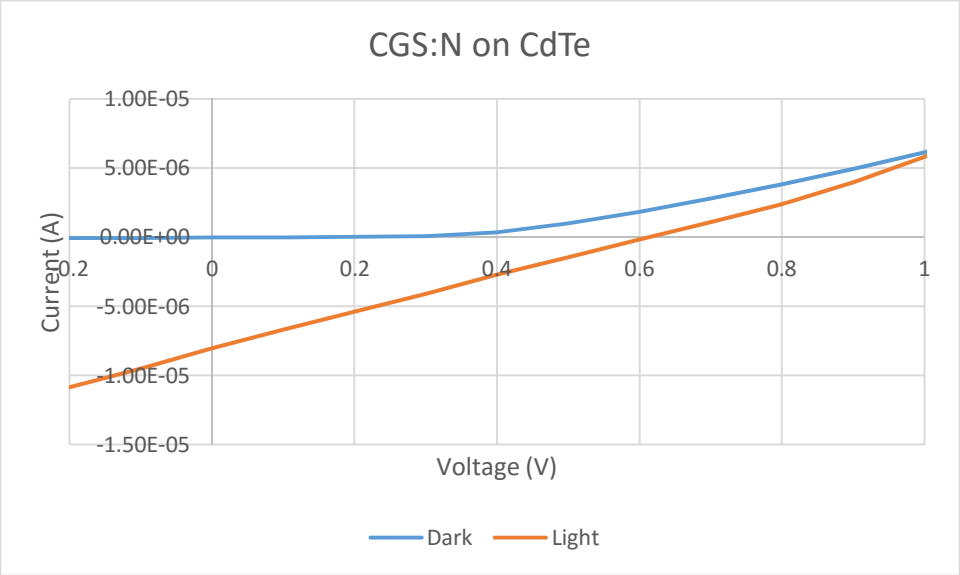

Figure 4.14: Light and Dark curves for a CdTe device using a CGS back contact

CHAPTER 5

CONCLUSIONS

Nitrogen was successfully added to CIS thin films. Nitrogen was detected through 2 separate methods that agreed within experimental error. The uptake of nitrogen was controlled and varied similarly in samples grown on both glass and Si substrates. The addition of nitrogen did not disrupt the growth of polycrystalline CIS films significantly, which are the kinds of films that would be used in devices. The addition of nitrogen does not form any new crystalline phases detectable with XRD, and does not have a consistent effect on overall film stoichiometry, besides replacing Se.

The resulting films were highly conductive, with a 4 order of magnitude decrease in resistivity from undoped films. Nitrogen apparently did act as a p-type acceptor. The lowest conductivity films had resistivities of around 1 Ohm-cm, higher than typical transparent conducting oxides.

CHAPTER 6

REFERENCES

[1] Fraunhofer Institute for Solar Energy Systems, ISE, "Photovoltaics Report," 6 June 2016.

[2] S. Narasimha, A. Rohatgi, and A. W. Weeber, "An optimized rapid aluminum back surface field technique for silicon solar cells," *IEEE Trans. Electron. Devices*, vol. 46, no. 7, pp. 1363–1370, July 1999.

[3] H. Neff, P. Lange, M. L. Fearheiley, and K. J. Bachmann, "Optical and electrochemical properties of CuInSe2 and CuInS2-CuInSe2 alloys," *Appl. Phys. Lett.*, vol. 47, 15 November 1985, p. 1089, 1985.

[4] K.-A. Kim, K.-B. Song, J. Kim, and K. Cho, "Chalcogen-based thin film transistor using $CuInSe_2$ photo-active layer," *Curr. Appl. Phys.*, vol. 9, no. 6, pp. 1326–1329, November 2009.

[5] M. Nishitani, T. Negami, S. Kohiki, M. Terauchi, T. Wada, and T. Hirao, "Homojunction diode of CuInSe2 thin film fabricated by nitrogen implantation," *J. Appl. Phys.*, vol. 74, no. 3, pp. 2067–2070, August 1993.

[6] E. Fortunato, P. Barquinha, and R. Martins, "Oxide Semiconductor Thin-Film Transistors: A Review of Recent Advances," *Adv. Mater.*, vol. 24, no. 22, pp. 2945–2986, Jun. 2012.

[7] M. A. Green, K. Emery, Y. Hishikawa, W. Warta, and E. D. Dunlop, "Solar cell efficiency tables (version 47)," *Prog. Photovolt: Res. Appl.*, vol. 24:, no. 1, pp. 3–11, January 2016.

[8] W. Shockley and H. J. Queisser, "Detailed Balance Limit of Efficiency of pn Junction Solar Cells," J. Appl. Phys., vol. 32, 510 (1961); doi: 10.1063/1.1736034.

[9] M. A. Green, “Limits on the open-circuit voltage and efficiency of silicon solar cells imposed by intrinsic Auger processes,” *IEEE Trans. Electron. Devices*, vol. ED-31, no. 5, pp. 671–678, May 1984.

[10] K. Kato, A. Murata, and K. Sakuta, “Energy pay-back time and life-cycle CO_2 emission of residential PV power system with silicon PV module,” *Prog. Photovolt: Res. Appl.*, vol. 6:, no. 2, pp. 105–115 doi:10.1002/(SICI)1099-159X(199803/04)6:2<105::AID-PIP212>3.0.CO;2-C.

[11] K. E. Knapp and T. L. Jester, “An Empirical Perspective on the Energy Payback Time for Photovoltaic Modules,” Solar 2000 Conference, 16 June 2000.

[12] S. H. Demtsu and J. R. Sites, “Effect of back-contact barrier on thin-film CdTe solar cells,” *Thin Solid Films*, vol. 510, Issues 1–2, pp. 320–324, 3 July 2006.

[13] A. O. Pudov, M. Gloeckler, S. H. Demtsu, J. R. Sites, K. L. Barth, R. A. Enzenroth, and W. S. Sampath, “Effect of back- contact copper concentration on CdTe cell operation" Proceedings of the 29th IEEE Photovoltaic Specialists Conference, pp. 2–5.

[14] T. Wada, N. Kohara, S. Nishiwaki, and T. Negami, “Characterization of the Cu(In,Ga)Se2/Mo interface in CIGS solar cells,” *Thin Solid Films*, vol. 387, no. 1, pp. 118–122, 29 May 2001.

[15] T. Dullweber, O. Lundberg, J. Malmstrom, M. Bodegard, L. Stolt, U. Rau, H. W. Schock, and J. H. Werner, “Back surface band gap gradings in Cu(In,Ga) Se_2 solar cells,” *Thin Solid Films*, vol. 387, no. 11–13, pp. 13–15, 2001.

[16] M. A. Green, K. Emery, Y. Hishikawa, W. Warta, and E. D. Dunlop, “Solar cell efficiency tables (version 39),” *Prog. Photovolt: Res. Appl.*, vol. 20, no. 1, pp. 12–20, Jan. 2012.

[17] D. Liao and A. Rockett, "Cd doping at the $CuInSe_2$/CdS heterojunction," *J. Appl. Phys.*, vol. 93, no. 11, pp. 9380–9382, 2003; http://dx.doi.org/10.1063/1.1570500

[18] M. A. Contreras, M. J. Romero, B. To, F. Hasoon, R. Noufi, S. Ward, and K. Ramanathan, "Optimization of CBD CdS process in high-efficiency $Cu(In,Ga)Se_2$-based solar cells," *Thin Solid Films*, vol. 403-404, pp. 204–211, 1 February 2002.

[19] E. Colegrove, R. Banai, C. Blissett, C. Buurma, J. Ellsworth, M. Morley, S. Barnes, C. Gilmore, J. D. Bergeson, R. Dhere, M. Scott, T. Gessert, and S. Sivananthan, "High-Efficiency Polycrystalline CdS/CdTe Solar Cells on Buffered Commercial TCO-Coated Glass.," J. Electronic Materials, vol. 41, no. 10, pp. 2833, 2012

[20] P. Jackson, D. Hariskos, R. Wuerz, O. Kiowski, A. Bauer, T. M. Friedlmeier, and M. Powalla, "Properties of $Cu(In,Ga)Se_2$ solar cells with new record efficiencies up to 21.7%," *Phys. status solidi - Rapid Res. Lett.*, vol. 9, no. 1, pp. 28–31, January 2015.

[21] S. Kwon, D. Lee, B. Ahn, K Yoon, and J. Song, "Characterization of Cu $(In_{1-x}Ga_x)Se_2$ Films Prepared by Three-Stage Coevaporation and Their Application to CIGS Solar Cells for a 14.48% Efficiency," *J. Korean Physical Society*, vol. 39, no. 4, pp. 655–660, October 2001.

[22] R. Wuerz, A. Eicke, M. Frankenfeld, F. Kessler, M. Powalla, P. Rogin, and O. Yazdani-Assl, "CIGS thin-film solar cells on steel substrates," *Thin Solid Films*, vol. 517, no. 7, pp. 2415–2418, 2 February 2009.

[23] V. K. Kapur, A. Bansal, P. Le, O. Asensio, and N. Shigeoka, "Non-vacuum processing of CIGS solar cells on flexible polymer substrates," Proceedings of 3rd World Conference on *Photovoltaic Energy Conversion*, Osaka, Japan, 2003, pp. 465–468 Vol.1.

[24] C. H. Chang, A. Davydov, B. J. Stanbery, and T. J. Anderson, "Thermodynamic assessment

of the Cu-In-Se system and application to thin film photovoltaics," in *Conference Record of the Twenty Fifth IEEE Photovoltaic Specialists Conference - 1996*, 13 May 1996, pp. 849–852.

[25] R. N. Bhattacharya, J. F. Hiltner, W. Batchelor, M. A. Contreras, R. N. Noufi, and J. R. Sites, "15.4% $CuIn_{1-x}Ga_xSe_2$-Based Photovoltaic Cells from Solution-Based Precursor Films," European Materials Research Society Meeting, Strasbourg, France, 1 June 1999.

[26] A. Rockett, T. C. Lommasson, P. Campos, L. C. Yang, and H. Talieh, "Growth of $CuInSe_2$ by two magnetron sputtering techniques," *Thin Solid Films*, vol. 171, no. 1, 1 April 1989.

[27] N. B. Singh, R. H. Hopkins, and J. D. Feichtner, "Effect of annealing on the optical quality of $AgGaS_2$ and $AgGaSe_2$ single crystals," *J. Mater. Sci.*, vol. 21, no. 3, pp. 837–841, 1986.

[28] S. B. Zhang, S. Wei, and A. Zunger, "Elements of doping engineering in semiconductors," AIP Conf. Proc. vol. **462**, no. 62 (1999); 9 September 1998.

[29] S. Roy, P. Guha, S. Chaudhuri, and A. K. Pal, "$CuInTe_2$ thin films synthesized by graphite box annealing of In/Cu/Te stacked elemental layers," *Vacuum*, vol. 65, no. 1, pp. 27–37, 26 February 2002.

[30] A. S. Poplavnoi, Y. I. Polygalov, and A. M. Ratner, "Energy band structure of the compounds $AgGaS_2$, $AgGaSe_2$, and $AgGaTe_2$," *Soviet Physics Journal*, vol. 17, no. 11, pp. 1495-1499, November 1974.

[31] H. F. Myers, C. H. Champness, and I. Shih, "Electrical effect of introducing elemental sodium into the Bridgman melt of $CuInSe_{2+x}$ crystals," *J. Cryst. Growth*, vol. 387, pp. 36–40, 1 February 2014.

[32] S. M. Wasim, "Transport properties of $CuInSe_2$," *Sol. Cells*, vol. 16, pp. 289–316, January-

February 1986.

[33] J. Parkes, R. D. Tomlinson and M. J. Hampshire, “Electrical properties of $CuInSe_2$ single crystals,” Solid-State Electronics, vol. 16, no. 7, pp. 773–777, July 1973.

[34] J. Lim, J. Choi, and I. Choi, “Characteristics of $CuInSe_2$ Thin Films Prepared by Sputtering of a Cu_2Se-In_2Se_3 Target,” J. Korean Phys. Soc., vol. 30, no. 2, pp. 293–298, April 1997.

[35] J. Piekoszewski, J.J. Loferski, R. Beaulieu, J. Beall, B. Roessler, and J. Shewchun, “RF-sputtered $CuInSe_2$ thin films,” *Sol. Energy Mater.*, vol. 2, no. 3, pp. 363–372, April-June 1980.

[36] D. J. Schroeder, J. L. Hernandez, G. D. Berry, and A. A. Rockett, “Hole transport and doping states in epitaxial CuIn(1-x)Ga(x)Se(2),” *J. Appl. Phys.*, vol. 83, no. 3, pp. 1519–1526, 1998.

[37] S. P. Grindle, A. H. Clark, S. Rezaie-Serej, E. Falconer, J. McNeily, and L. L. Kazmerski, “Growth of $CuInSe_2$ by molecular beam epitaxy,” *J. of Appl. Phys.*, vol. 51, no. 10. pp. 5464–5469, 1980.

[38] S. Chichibu, “Room-temperature near-band-edge photoluminescence from $CuInSe_2$ heteroepitaxial layers grown by metalorganic vapor phase epitaxy,” Appl. Phys. Lett., vol. 70, no. 14, pp. 1840, 1997.

[39] D. J. Schroeder, “Effects of Intrinsic and Extrinsic Point Defects on Epitaxial Single Crystal Copper-Indium(1-X)-Gallium(x)-Diselenide ,” Thesis (Ph.D.)--University of Illinois at Urbana-Champaign, 1997.

[40] A. Rockett, “The effect of Na in polycrystalline and epitaxial single-crystal $CuIn_{1-x}Ga_xSe_2$,” *Thin Solid Films*, vol. 480–481, pp. 2–7, 1 June 2005.

[41] D. J. Schroeder and A. A. Rockett, “Electronic effects of sodium in epitaxial $CuIn_{1-x}Ga_xSe_2$,” *J. Appl. Phys.*, vol. 82, no. 10, p. 4982, 1997.

[42] U. Rau, K. Taretto, and S. Siebentritt, “Grain boundaries in $Cu(In,Ga)(Se,S)_2$ thin-film solar cells,” *Appl. Phys. A-Materials Sci. Process.*, vol. 96, no. 1, pp. 221–234, 3 December 2008.

[43] S. Kohiki, M. Nishitani, T. Negami, K. Nishikura, and T. Hirao, “Nitrogen implantation for molecular beam deposited $CuInSe_2$ thin films,” *Appl. Phys. Lett.*, vol. 59, no. 14, pp. 1749–1751, 8 July 1991.

[44] M. Nishitani, T. Negami, M. Terauchi, T. Wada, and T. Hirao, “Fabrication of P-Type Cuinse2 Thin Film by MBD Using ECR Excited Nitrogen Ion Source,” *MRS Proceedings*, vol. 268, 1992.

[45] J. Qiu, J. M. DePuydt, H. Cheng, and M. A. Haase, “Heavily doped p-ZnSe:N grown by molecular beam epitaxy,” *Appl. Phys. Lett.*, vol. 59, no. 23, pp. 2992–2994, 1991.

[46] E. Tournié, P. Brunet, and J. P. Faurie, “p-Type doping of ZnSe and related materials controlled by diluting nitrogen in an inert gas,” *J. Cryst. Growth*, vol. 201-202, pp. 938–941, May 1999.

[47] S. Gundel, D. Albert, J. Nürnberger, and W. Faschinger, “Stability of nitrogen in ZnSe and its role in the degradation of ZnSe lasers,” *Phys. Rev. B*, vol. 60, no. 24, pp. R16271–R16274, 15 December 1999.

[48] A. Rockett, T. C. Lommasson, P. Campos, L. C. Yang, and H. Talieh, “Growth of CuInSe2 by two magnetron sputtering techniques,” *Thin Solid Films*, Volume 171, Issue 1, Pages 109-123, 1 April 1989.

[49] L.-C. Yang, H. Z. Mao, A. Rockett, W. N. Shafarman, and R. W. Birkmire, “The growth by the hybrid sputtering and evaporation method and microstructural studies of CuInSe2 films,” *Sol. Energy Mater. Sol. Cells*, vol. 36, no. 4, pp. 445–455, 1995.

[50] R. H. Packwood and J. D. Brown, "A Gaussian expression to describe φ(ρz) curves for quantitative electron probe microanalysis," *X-Ray Spectrometry,* Volume 10, Issue 3, pages 138–146, July 1981

[51] D. Liao and a. Rockett, “Epitaxial growth of Cu(In,Ga)Se 2 on GaAs(110),” *J. Appl. Phys.*, vol. 91, no. 3, pp. 1978–1983, 2002.

[52] C. A. Mullan, C. J. Kiely, M. V. Yakushev, M. Imanieh, R. D. Tomlinson, and A. Rockett, “The effects of ion implantation on the microstructure of $CuInSe_2$ single crystals,” *Philosophical Magazine A,* Volume 73, Issue 4, 1996 2006.

[53] S. Niki, P. J. Fons, a. Yamada, Y. Lacroix, H. Shibata, H. Oyanagi, M. Nishitani, T. Negami, and T. Wada, “Effects of the surface $Cu_{2-x}Se$ phase on the growth and properties of CuInSe2 films,” *Appl. Phys. Lett.*, vol. 74, no. 11, pp. 1630–1632, 1999.